

Criterion for fingering instabilities in colloidal gels

Thibaut Divoux,^{1,2} Asheesh Shukla,¹ Badis Marsit,³ Yacouba Kaloga,¹ and Irmgard Bischofberger³

¹*MultiScale Material Science for Energy and Environment, UMI 3466, CNRS-MIT, 77 Massachusetts Avenue, Cambridge, Massachusetts 02139, USA*

²*Department of Civil and Environmental Engineering,*

Massachusetts Institute of Technology, Cambridge, MA 02139

³*Department of Mechanical Engineering, Massachusetts Institute of Technology, Cambridge, MA 02139*

(Dated: February 18, 2020)

We sandwich a colloidal gel between two parallel plates and induce a radial flow by lifting the upper plate at a constant velocity. Remarkably, two distinct scenarios result from such a tensile test: (i) stable flows during which the gel undergoes a tensile deformation without yielding and (ii) unstable flows characterized by the radial growth of air fingers into the gel. We show that the transition to the unstable regime is observed beyond a critical rate of viscous energy dissipation in the bulk that is proportional to the gel's yield stress. The most unstable wavelength of the patterns exhibits the characteristic scalings of the classical viscous fingering instability, independent of the yield stress, indicating a full fluidization of the gel. Our work provides a quantitative criterion for the onset of fingering in colloidal gels, and sheds new light on their shear-induced yielding transition.

The displacement of a more viscous fluid by a less viscous one in a confined geometry can induce the formation of complex patterns [1–3]. Even in the simplest case of two Newtonian fluids, this viscous fingering instability keeps yielding new discoveries [4–10]. When the displaced fluid is replaced with a non-Newtonian one, the finger growth dynamics can be significantly altered [11–18]. For instance, in the displacement of a viscoelastic fluid by a Newtonian one, a transition from viscous fingering to fracture occurs above a critical Deborah number, driven by the release of elastic stresses [19–24]. While a consensus has been reached for the mechanism responsible for this transition in viscoelastic fluids with a finite relaxation timescale, we are far from a comprehensive description of fingering instabilities in another class of complex materials, yield stress fluids, which exhibit a solid-like behavior at rest and a solid-to-liquid transition beyond a critical stress σ_c [25–27]. In dense foams and emulsions displaced by air, for example, the pattern morphology associated with fingering instabilities is strongly rate-dependent [28, 29]. In tensile tests of dense microgels, where the samples are sandwiched between two parallel plates that get separated at a constant velocity, the yield stress can suppress the instability [30]. The transition between stable and unstable displacement lacks a theoretical explanation, but is thought to be linked to the sample adhesion to the plates [30, 31]. Finally, the parameter governing the most unstable wavelength of the pattern in the unstable displacement has been alternatively reported as being set by the yield stress, or being independent of the yield stress [29, 32, 33], which calls for more experimental investigations.

In this Letter, we report a comprehensive description of both the criterion for stabilization and the characteristics of the most unstable wavelength for a colloidal gel displaced by air. We confine the gel in a parallel-plate geometry of initial gap thickness h_0 and set it into motion

by lifting the upper plate at a constant lift velocity v_l . We show that the onset of the viscous fingering instability occurs at a critical rate of viscous energy dissipation, beyond which the gel yields locally allowing for the radial growth of fingers. Remarkably, the most unstable wavelength λ_c obeys the scaling with v_l and h_0 of a Newtonian fluid, which indicates a rapid and complete fluidization of the gel at the locus where fingers grow. This observation is confirmed by the power-law scaling of the normal force relaxation occurring during the tensile test. Our results provide a comprehensive framework for fingering instabilities in colloidal gels and reveal a novel control parameter for the gels' shear-induced yielding transition.

The colloidal gel consists of carbon black particles (Vulcan XC72R, Cabot) of typical size $0.5 \mu\text{m}$ suspended at weight fractions ranging from 4% to 10% wt. in light mineral oil (Sigma Aldrich; viscosity $\eta_s = 20 \text{ mPa}\cdot\text{s}$, density $\rho_s = 0.838 \text{ g/ml}$). Due to attractive van der Waals forces [34, 35], carbon black particles form a space-spanning gel network, whose linear viscoelastic properties are characterized by a frequency-independent elastic response [36–39]. Under external stresses lower than the yield stress σ_c , the gel behaves as a solid. For $\sigma > \sigma_c$, the gel flows. This shear-induced yielding transition is time-dependent, spatially heterogeneous and characterized by activated dynamics [38–42]. Here, we place a 8% wt. carbon black gel in a stainless steel parallel-plate geometry (diameter $2R = 40 \text{ mm}$ or 60 mm), whose upper plate is connected to a stress-controlled rheometer (DHR-3, TA Instruments). The temperature of the lower plate is fixed to 25°C by Peltier elements. To account for the high sensitivity of carbon black gels on shear history [43–45], the sample is fully fluidized prior to each test by applying a large shear stress $\sigma = 100 \text{ Pa}$ for 30 s. The stress is subsequently swept down to $\sigma = 0 \text{ Pa}$ at a rate of 1 Pa/s while the gel reforms. This protocol yields a reproducible initial state [44]. The resulting viscoelastic moduli G'_0 and

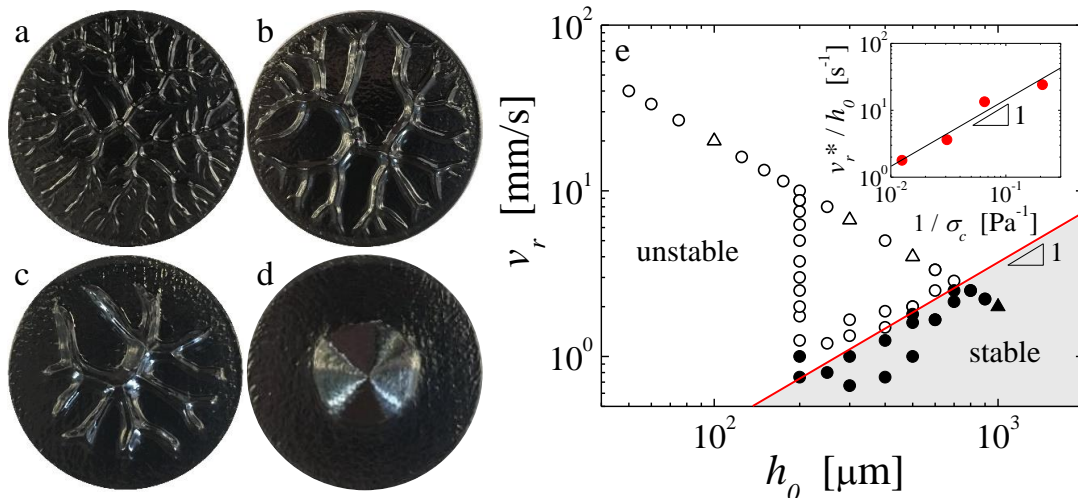


Figure 1: (a)–(d) Patterns obtained at a fixed lift velocity $v_l = 200 \mu\text{m/s}$ for increasing initial gap thicknesses $h_0 = 100, 300, 500$ and $900 \mu\text{m}$ in tensile tests performed with a 8% wt. carbon black gel placed between two parallel plates of diameter $2R = 40 \text{ mm}$. (e) Stability diagram: radial velocity v_r versus initial gap thickness h_0 . Closed symbols denote stable conical patterns, open symbols denote unstable fingering patterns. The data points corresponding to the four images are indicated as triangles. The red line denotes the critical velocity v_r^* separating the stable from the unstable regime. Inset: critical velocity normalized by the initial gap thickness v_r^*/h_0 versus the inverse of the yield stress σ_c^{-1} for carbon black gels of four different concentrations 4%, 6%, 8% and 10% wt. The yield stress is determined as the crossover of G' and G'' during a stress sweep from 1 Pa to 100 Pa, at a frequency of $f = 1 \text{ Hz}$, with a waiting time of 5 s per point.

G''_0 of the gel at rest are determined during 1 min by small amplitude oscillations (strain amplitude $\gamma = 0.1\%$, frequency $f = 1 \text{ Hz}$) [Fig. S1 in Supplemental Material]. We then perform a tensile test at a constant lift velocity v_l during which we record the normal force F_N . The plate separation yields a roughly symmetric pattern on both plates, which is photographed.

Two main types of patterns occur in the tensile tests, depending on the lift velocity v_l and the initial gap thickness h_0 : (i) unstable patterns characterized by highly branched structures [Fig. 1(a)–(c)], and (ii) stable patterns characterized by conical piles of carbon black gel at the center of the plates [Fig. 1(d)]. Unstable patterns result from instabilities at the air/gel interface at the periphery of the parallel plate geometry and are observed for high lift velocities and small initial gap thicknesses. Air fingers grow into the gel along the radial direction leaving behind regions depleted in gel. Stable patterns result from a stable displacement of the gel under the tensile flow generated by the plate separation, and occur for low lift velocities and large initial gap thicknesses. Such stable patterns do not occur in Newtonian fluids, but were reported in soft glassy materials such as dense microgels and mortar pastes [17, 30]. Our observations are summarized in a stability diagram, where we report the radial velocity $v_r = v_l(R/2h_0)$, which is the velocity for radial air invasion, and the initial gap thickness h_0 [Fig. 1(e)]. The transition from unstable to stable displacement occurs at a critical radial velocity v_r^* , which increases linearly with increasing h_0 . Such a scaling is

robustly observed for different concentrations of carbon black ranging from 4% to 10% wt. [Fig. S2 in Supplemental Material]. Surprisingly, the stability boundary $v_r^*(h_0)$ shifts towards lower velocity values for carbon black gels with larger particle concentration. Counter intuitively, stronger gels exhibit unstable patterns over a larger range of v_r and h_0 . From our additional experiments on gels with 4%, 6% and 10% wt. we find $v_r^*/h_0 \propto \sigma_c^{-1}$, as shown in the inset of Fig. 1(e). The physical meaning of this scaling becomes evident when re-written as a constant rate of energy dissipation per unit volume \mathcal{P}_d , dissipated at the onset of the yielding transition: $\mathcal{P}_d = \sigma_c \dot{\gamma}^* = \text{const.}$, where $\dot{\gamma}^* \simeq v_r^*/h_0$ denotes the critical shear rate below which the flow induced by the plate separation is stable. Air fingers grow into the gel only if the mechanical energy provided to the gel by the plate separation leads to viscous dissipation over a timescale that is shorter than the time needed for the gel to heal.

To get further evidence for this scenario, we consider the evolution of the normal force $F_N(h)$ during plate separation at $v_l = 200 \mu\text{m/s}$ for an unstable pattern with $h_0 = 200 \mu\text{m}$ and a stable pattern with $h_0 = 1000 \mu\text{m}$. In both cases, F_N exhibits a sharp increase up to a maximum followed by a two-step relaxation characterized by two power laws with respective exponents α and β , as shown in Fig. 2(a). For the unstable pattern, the first relaxation exhibits an exponent $\alpha \simeq 5$ that is characteristic of a purely Newtonian response [46–48]. Indeed, assuming a constant viscosity η , and integrating Darcy’s

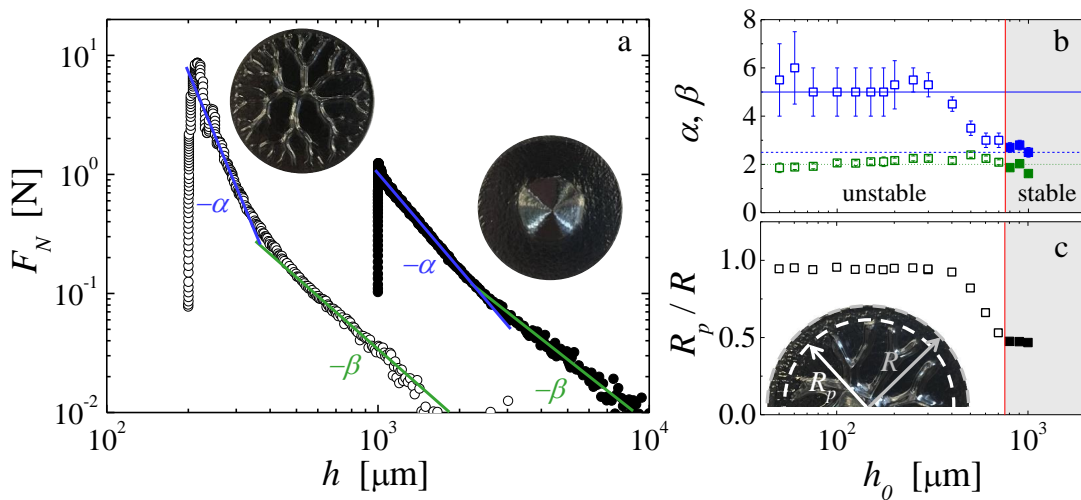


Figure 2: (a) Normal force F_N versus gap thickness h during a tensile test performed at a constant lift velocity $v_l = 200 \mu\text{m}$. The two curves correspond to two initial gap thicknesses: $h_0 = 200 \mu\text{m}$ resulting in viscous fingering (open symbols) and $h_0 = 1000 \mu\text{m}$ resulting in a stable conical deposit (closed symbols). The blue lines denote the power-law exponents of the first relaxation step: $\alpha = 5$ for $h_0 = 200 \mu\text{m}$ and $\alpha = 2.5$ for $h_0 = 1000 \mu\text{m}$. The green lines denote the power-law exponents of the second relaxation step: $\beta \simeq 2$ for both experiments. (b) Exponents α and β versus the initial gap thickness h_0 . With increasing gap thickness, α transitions from a Newtonian-like response ($\alpha = 5$ – blue continuous line) to a yield stress dominated behavior ($\alpha = 2.5$ – blue dashed line). β is roughly constant over the range of gap thickness explored ($\beta \simeq 2$ – green line). (c) The relative extent R_p/R of the pattern decreases upon the approach to the stable regime. Inset: definition of R and R_p . The vertical lines in (b) and (c) denote the boundary between the stable and the unstable regime.

law to compute the pressure field, which is in turn integrated over the area occupied by the material yields the expression $F_N(h) = 3\pi\eta R^4 h_0^2 v_l / 2h^5$ [32, 46]. The air fingers invade the gap radially and locally fluidize the gel into a viscous suspension. The second relaxation exhibits a power-law exponent $\beta \simeq 2$, which is characteristic of the necking of a viscous liquid [46] and corresponds to the extensional flow of the gel threads linking the crest of the branched pattern formed on the upper and lower plates.

By contrast, the early growth of the stable pattern is characterized by a first power-law relaxation step with an exponent $\alpha \simeq 2.5$, characteristic of a yield stress fluid [31, 32]. Indeed, assuming that the pressure gradient is balanced by the yield stress σ_c yields the expression $F_N(h) = 2\pi R^3 h_0^{3/2} \sigma_c / 3h^{5/2}$. While being dragged towards the center of the plates, the carbon black gel thus behaves predominantly as an elastic soft solid. The gel may rearrange to accommodate the extensional flow, but over timescales that are large compared to the gel’s “healing timescale” denoting the re-formation of the network, such that $G' > G''$ at all times. The second relaxation step exhibits a power law with an exponent $\beta \simeq 2$, as for the unstable case. Note that the transition from the first to the second relaxation regime occurs at a critical gap $h_c \simeq 2600 \mu\text{m}$ that coincides with reaching the final diameter of the deposit, as determined from mass conservation arguments, further confirming that the second relaxation step denotes the thinning of the gel thread

connecting the two cones of gel located on the lower and upper plates.

More generally, for tensile tests performed at a constant lift velocity, the first relaxation step of the normal force displays a Newtonian behavior characterized by $\alpha = 5$ at small h_0 . For increasing initial gap thicknesses approaching the boundary to the stable regime, α decreases monotonically until reaching $\alpha = 2.5$, the value expected for a yield stress fluid, at the onset of stable displacement, as shown in Fig. 2(b). Concomitantly, the pattern transitions from a highly branched structure that extends over the entire diameter $2R$ of the plate, to an unstable pattern of reduced size $2R_p$ within a transitional range of h_0 to finally a stable conical shape, as shown in Fig. 2(c). The second relaxation step of the normal force displays a power-law exponent $\beta \simeq 2$, for all initial gap thicknesses, whether the flow is unstable or not. These observations are robust and also observed in experiments at fixed initial gap thickness performed at various lift velocities [Fig. S3 in Supplemental Material].

As further proof that the carbon black gel is fully fluidized during the unstable pattern growth, we examine the most unstable wavelength characterizing the onset of the instability λ_c [49]. We find the wavelength to scale as $\lambda_c \propto h_0^{3/2}$ with the initial gap thickness for $h_0 > 200 \mu\text{m}$, and as $\lambda_c \propto v_r^{-1/2}$ with the radial velocity, as shown in Fig. 3. These two scaling laws are indeed in agreement with the predictions from a linear stability analysis for a Newtonian fluid with viscosity η and surface tension Γ

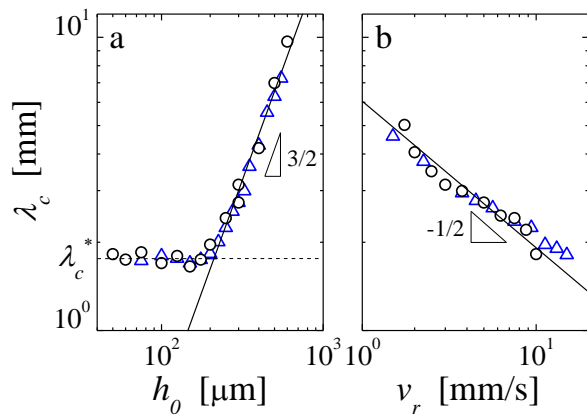


Figure 3: Most unstable wavelength λ_c of the fingering patterns versus (a) the initial gap thickness h_0 and (b) the radial velocity v_r . In (a), the solid line corresponds to a power-law exponent of $3/2$, the dashed line to $\lambda_c^* = 1.76$ mm. In (b), the line corresponds to a power-law exponent of $-1/2$. Data obtained with a 8% wt. carbon black gel and two different plate diameters $2R = 40$ mm (o) and 60 mm (Δ).

[2, 50]:

$$\lambda_c \simeq \sqrt{\frac{2\pi h_0^3 \Gamma}{\eta v_r R}} = \frac{\pi h_0}{\sqrt{\eta v_r / \Gamma}} \quad (1)$$

for plates with large aspect ratio $R/h_0 \gg 1$. This confirms that the yield stress plays a negligible role in the formation of the fingering patterns. Moreover, if we take for Γ the surface tension of the light mineral oil Γ_s , we obtain $\eta = 0.18$ Pa.s, which is compatible with the viscosity of a fully fluidized carbon black gel (measured at high shear rates $\dot{\gamma} = 1000$ s $^{-1}$ [39]). This viscosity is about a factor of 4 lower than the one extracted from the first relaxation step of the normal force. This is because the viscosity extracted from λ_c corresponds to the state of the gel at the very tip of the finger, whereas that extracted from the force relaxation is an average all along the length of the fingers. Remarkably, the most unstable wavelength saturates at a constant value $\lambda_c^* = 1.76 \pm 0.10$ mm for $h_0 < 200$ μ m [Fig. 3(a)]. Such saturation is unexpected. We note, however, that this value is compatible with the capillary length $\ell_c = \sqrt{\Gamma_s / (\rho_s g)} \simeq 1.8$ mm of the mineral oil, which suggests that the thinnest fingers that form during a tensile experiment are limited by capillary effects.

In summary, we show that the presence of attractive colloidal particles suspended in a Newtonian liquid can suppress the viscous fingering instability. We provide the criterion for the onset of the instability as a critical rate of energy dissipation \mathcal{P}_d below which the rapid healing of the gel network due to attractive interactions prevents the finger invasion. The gel continuously rearranges under shear but exhibits an elastic response at all times during the tensile test, which leads to the formation of

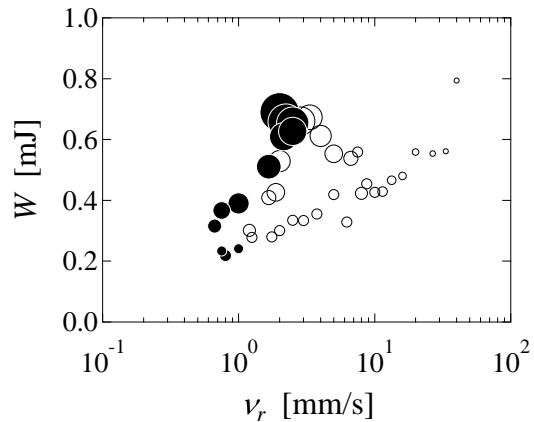


Figure 4: Energy W needed for plate separation versus the radial velocity v_r . Data obtained with a 8% wt. carbon black gel and plates of diameter $2R = 40$ mm. Increasing symbol size encodes the initial gap thickness h_0 ranging from 50 μ m to 1 mm. Open symbols denote unstable patterns, closed symbols denote stable patterns.

stable cones at the center of the plate. For $\mathcal{P} \gtrsim \mathcal{P}_d$, which is reached at large enough lift velocities or small enough initial gap thicknesses, the gel yields locally along the periphery of the plate. Air fingers invade the gap producing highly branched patterns that exhibit wavelengths and normal-force responses characteristic of Newtonian fluids, indicating that the gel is fully fluidized. Interestingly, this criterion is distinct from a simple criterion of an energy threshold. Indeed, the energy W needed to separate the two plates, calculated as the integral of the normal force from the initial gap thickness h_0 to plate separation, is not correlated with the transition from stable to unstable flow, as shown in Fig. 4.

More generally, the predominance of viscous dissipation governing the normal force response that we find in carbon black gels is in agreement with tensile tests performed with gels composed of clay particles [51]. Moreover, our observation that the fingering characteristics are set solely by the properties of the fully fluidized state of the sample might shed light on discrepancies pointed out in [32], where the finger width observed in hair gel solutions is independent of their yield stress. However, our results strongly contrast with experiments on jammed assemblies of soft particles such as dense microgels for which the wavelength of the pattern is set by the yield stress of the material [29]. This suggests that the mechanism for fingering in soft repulsive glasses is distinct from that of the gels studied here, which indicates that we should not look for a universal scenario describing viscous fingering in all yield stress fluids. Our work thus provides a novel scenario for the onset of cohesive failure in gels of attractive colloidal particles. Future work should aim at placing the criterion for fingering instabilities in the context of the activated-like yielding scenario

that currently prevails in the literature [52–54]. Within that framework, our findings could be relevant for interpreting recent yielding experiments in colloidal gels controlled by ultrasonic vibrations [55], and constitute a benchmark set of experimental data to test glassy constitutive models [56].

We thank S. Manneville, J.A. Dijksman, and G.H. McKinley for fruitful discussions. T.D. acknowledges support from the National Science Foundation under Grant No. NSF PHY 17-48958 through the KITP program on the Physics of Dense Suspensions. B.M. and I.B. acknowledge support from MIT MISTI-France.

-
- [1] P. G. Saffman and G. Taylor, *Proc. R. Soc. Lond. A* **245**, 312 (1958).
- [2] L. Paterson, *J. Fluid Mech.* **113**, 513 (1981).
- [3] J. D. Chen, *Exp. Fluids* **5**, 363 (1987).
- [4] D. Pihler-Puzović, P. Illien, M. Heil, and A. Juel, *Phys. Rev. Lett.* **108**, 074502 (2012).
- [5] I. Bischofberger, R. Ramachandran, and S. Nagel, *Nat. Commun.* **5**, 5265 (2014).
- [6] I. Bihi, M. Baudoin, J. E. Butler, C. Faille, and F. Zoueshtiagh, *Phys. Rev. Lett.* **117**, 034501 (2016).
- [7] H. S. Rabbani, D. Or, Y. Liu, C.-Y. Lai, N. B. Lu, S. S. Datta, H. A. Stone, and N. Shokri, *Proc. Natl. Acad. Sci. U.S.A.* **115**, 4833 (2018).
- [8] R. Alert, C. Blanch-Mercader, and J. Casademunt, *Phys. Rev. Lett.* **122**, 088104 (2019).
- [9] D. M. Escala, A. De Wit, J. Carballido-Landeira, and A. P. Muuzuri, *Langmuir* **35**, 4182 (2019).
- [10] T. E. Videbæk and S. R. Nagel, *Phys. Rev. Fluids* **4**, 033902 (2019).
- [11] J. Bohr, S. Brunak, and T. Noretranders, *Europhys. Lett.* **25**, 245 (1994).
- [12] K. V. McCloud and J. V. Maher, *Phys. Rep.* **260**, 139 (1995).
- [13] L. Kondic, M. J. Shelley, and P. Palfy-Muhoray, *Phys. Rev. Lett.* **80**, 1433 (1998).
- [14] A. Lindner, D. Bonn, E. C. Poiré, M. Ben Amar, and J. Meunier, *J. Fluid Mech.* **469**, 237256 (2002).
- [15] N. Puff, G. Debrégeas, J.-M. di Meglio, D. Higgins, D. Bonn, and C. Wagner, *Europhys. Lett.* **58**, 524 (2002).
- [16] A. Shaukat, Y. M. Joshi, and A. Sharma, *Ind. Eng. Chem. Res.* **48**, 8211 (2009).
- [17] Y. O. Mohammed Abdelhaye, M. Chaouche, J. Chapuis, E. Charlaix, J. Hinch, S. Roux, and H. Van Damme, *Eur. Phys. J. E* **35**, 45 (2012).
- [18] H. Van Damme, S. Mansoutre, P. Colombet, C. Lesaffre, and D. Picart, *C. R. Physique* **3**, 229 (2002).
- [19] E. Lemaire and H. Van Damme, *C.R. Acad. Sci. Paris* **309**, 859 (1989).
- [20] E. Lemaire, P. Levitz, G. Daccord, and H. Van Damme, *Phys. Rev. Lett.* **67**, 2009 (1991).
- [21] H. Zhao and J. V. Maher, *Phys. Rev. E* **47**, 4278 (1993).
- [22] S. Mora and M. Manna, *Phys. Rev. E* **81**, 026305 (2010).
- [23] G. Foyart, L. Ramos, S. Mora, and C. Ligoure, *Soft Matter* **9**, 7775 (2013).
- [24] C. Ligoure and S. Mora, *Rheol. Acta* **52**, 91 (2013).
- [25] P. Coussot, *J. Non-Newtonian Fluid Mech.* **211**, 31 (2014).
- [26] D. Bonn, M. M. Denn, L. Berthier, T. Divoux, and S. Manneville, *Rev. Mod. Phys.* **89**, 035005 (2017).
- [27] P. Coussot, *Rheol. Acta* **57**, 1 (2018).
- [28] S. S. Park and D. J. Durian, *Phys. Rev. Lett.* **72**, 3347 (1994).
- [29] A. Lindner, P. Coussot, and D. Bonn, *Phys. Rev. Lett.* **85**, 314 (2000).
- [30] Q. Barral, G. Ovarlez, X. Chateau, J. Boujlel, B. Rabideau, and P. Coussot, *Soft Matter* **6**, 1343 (2010).
- [31] P. Coussot, *J. Fluid Mech.* **380**, 363 (1999).
- [32] D. Derks, A. Lindner, C. Creton, and D. Bonn, *J. Appl. Phys.* **93**, 1557 (2003).
- [33] N. Maleki-Jirsaraei, A. Lindner, S. Rouhani, and D. Bonn, *J. Phys. Condens. Matter* **17**, S1219 (2005).
- [34] M. van der Waarden, *J. Colloid Sci.* **5**, 317 (1950).
- [35] P. A. Hartley and G. D. Parfitt, *Langmuir* **1**, 651 (1985).
- [36] V. Trappe and D. A. Weitz, *Phys. Rev. Lett.* **85**, 449 (2000).
- [37] V. Prasad, V. Trappe, A. D. Dinsmore, P. N. Segre, L. Cipelletti, and D. A. Weitz, *Faraday Discuss.* **123**, 1 (2003).
- [38] T. Gibaud, D. Frelat, and S. Manneville, *Soft Matter* **6**, 3482 (2010).
- [39] V. Grenard, T. Divoux, N. Taberlet, and S. Manneville, *Soft Matter* **10**, 1555 (2014).
- [40] J. Sprakel, S. Lindström, T. Kodger, and D. Weitz, *Phys. Rev. Lett.* **106**, 248303 (2011).
- [41] C. Perge, N. Taberlet, T. Gibaud, and S. Manneville, *J. Rheol.* **58**, 1331 (2014).
- [42] T. Gibaud, C. Perge, S. B. Lindström, N. Taberlet, and S. Manneville, *Soft Matter* **12**, 1701 (2016).
- [43] G. Ovarlez, L. Tocquer, F. Bertrand, and P. Coussot, *Soft Matter* **9**, 5540 (2013).
- [44] A. Helal, T. Divoux, and G. H. McKinley, *Phys. Rev. Applied* **6**, 064004 (2016).
- [45] J. B. Hipp, J. J. Richards, and N. J. W. Wagner, *J. Rheol.* **63**, 423 (2019).
- [46] J. J. Bikerman, *J. Colloid Sci.* **2**, 163 (1947).
- [47] D. Maugis, “Adherence and fracture mechanics,” (1991) Chap. 11, pp. 303–335.
- [48] A. Lindner, D. Derks, and M. J. Shelley, *Phys. Fluids* **17**, 072107 (2005).
- [49] The most unstable wavelength λ_c is determined by counting the number of fingers along the periphery of the plate. The underlying assumption that the pattern at the plate periphery is representative of the early stage of the experiment is justified as the short healing time of the gel, and the gel’s solid-like behavior at rest, allow for the early-stage pattern to be frozen in and to remain unchanged from the time of formation. Note that a direct visualization of the early stage is not possible because carbon black gels are optically opaque and leave a thin layer of gel adhered to the plates.
- [50] M. J. Shelley, F.-R. Tian, and K. Wlodarski, *Nonlinearity* **10**, 1471 (1997).
- [51] Y. O. Mohammed Abdelhaye, M. Chaouche, and H. van Damme, *App. Clay Sci.* **42**, 163 (2008).
- [52] L. Bocquet, A. Colin, and A. Ajdari, *Phys. Rev. Lett.* **103**, 036001 (2009).
- [53] S. M. Fielding, M. E. Cates, and P. Sollich, *Soft Matter* **5**, 2378 (2009).
- [54] S. Lindström, T. Kodger, J. Sprakel, and D. Weitz, *Soft*

Matter **8**, 3657 (2012).

- [55] T. Gibaud, N. Dagès, P. Lidon, L. C. A. G. Jung, M. Sztucki, A. Poulesquen, N. Hengl, F. Pignon, and S. Manneville, *Phys. Rev. X* **10**, 011028 (2020).
- [56] S. M. Fielding, “Elastoviscoplastic rheology and ageing in a simplified soft glassy constitutive model,” [ArXiv:1911.12340](https://arxiv.org/abs/1911.12340).

Criterion for fingering instabilities in colloidal gels

Supplemental Material

LINEAR VISCOELASTIC PROPERTIES OF CARBON BLACK GELS

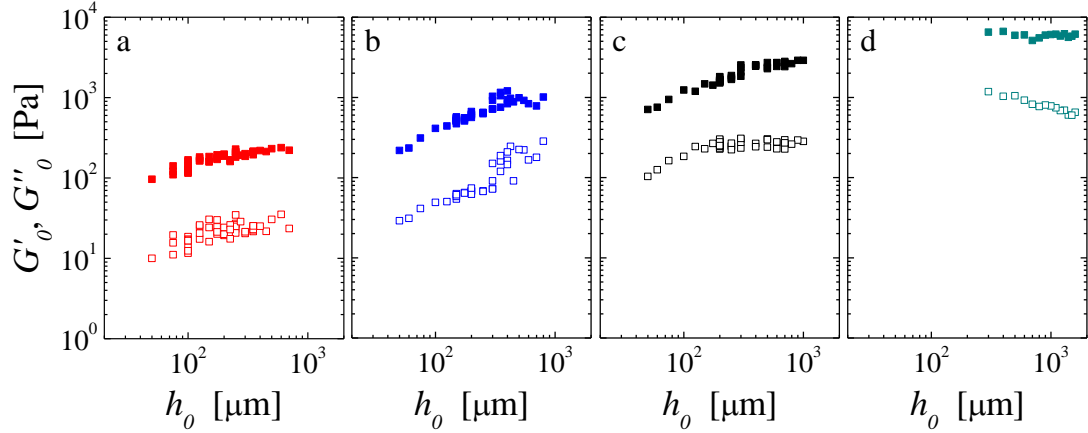


Figure S1: Linear viscoelastic moduli G'_0 (■) and G''_0 (□) versus the initial gap thickness h_0 for carbon black gels of four different concentrations: 4%, 6%, 8% and 10% wt. from (a) to (d). Measurements are performed under an imposed shear strain $\gamma_0 = 0.1\%$ at a frequency $f = 1$ Hz. Prior to each measurement, the sample is fully fluidized by imposing a large preshear at a stress $\sigma = 100$ Pa for 30 s. The gel reforms during a stress sweep from 100 Pa down to 0 Pa at constant rate ($1 \text{ Pa}\cdot\text{s}^{-1}$). The linear viscoelastic moduli are measured for 60 s and we report the average values over the last 30 s.

STABILITY DIAGRAM FOR GELS OF DIFFERENT CONCENTRATIONS

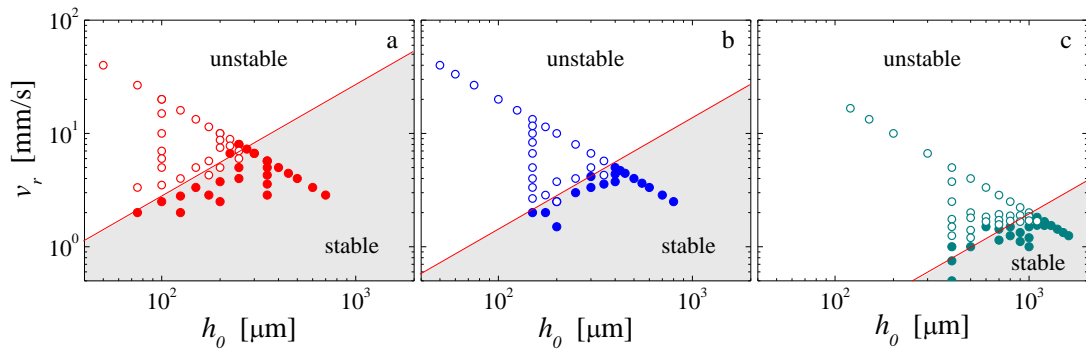


Figure S2: Stability diagram reporting the radial velocity v_r versus the initial gap thickness h_0 for tensile tests performed with carbon black gels of concentrations 4%, 6% and 10% wt. from (a) to (c). The red line denotes the critical velocity $v_r^*(h_0)$ separating the stable from the unstable regime. The boundary between stable and unstable flow shifts towards lower velocities with increasing carbon black concentration.

NORMAL FORCE RELAXATION AT DIFFERENT LIFT VELOCITIES

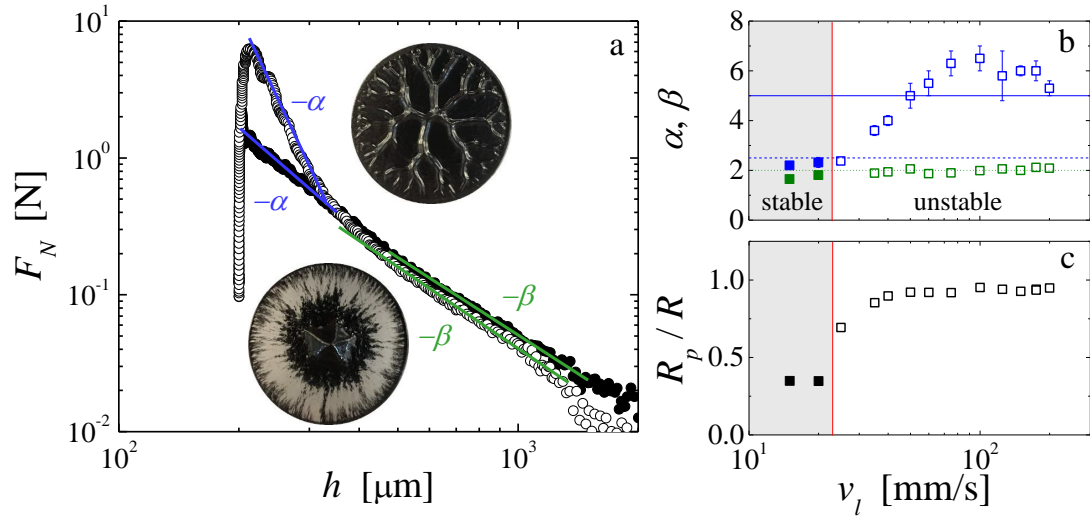


Figure S3: (a) Normal force F_N versus gap thickness h during a tensile test performed at two different lift velocities $v_l = 20 \mu\text{m/s}$ (closed symbols) and $100 \mu\text{m/s}$ (open symbols) in a parallel plate geometry of diameter $2R = 40$ mm. The blue lines denote the power-law exponents of the first relaxation step: $\alpha \simeq 2.5$ for $v_l = 20 \mu\text{m/s}$ and $\alpha \simeq 5$ for $v_l = 100 \mu\text{m/s}$. The green lines denote the power-law exponents of the second relaxation step: $\beta \simeq 2$ for both experiments. (b) Exponents α and β versus the lift velocity v_l . With increasing lift velocity, α transitions from a yield stress dominated behavior ($\alpha = 2.5$ – blue dashed line) to a Newtonian-like response ($\alpha = 5$ – blue continuous line). β is roughly constant over the range of lift velocities explored ($\beta \simeq 2$ – green line). (c) The relative extent R_p/R of the pattern versus v_l . The vertical lines in (b and c) denote the boundary between the stable and the unstable regime.